Received 28 March 2025; accepted 20 June 2025. Date of publication 30 June 2025; date of current version 6 November 2025.

Digital Object Identifier 10.1109/OJAP.2025.3584242

An Effective Approach to Scattering From Parallel Cylinders Above a Planar Conducting Surface

RENAT ABDULLIN [1] (Graduate Student Member, IEEE), GIADA M. BATTAGLIA [1], ANDREA F. MORABITO [1] (Senior Member, IEEE), LORENZO CROCCO [2] (Senior Member, IEEE), TOMMASO ISERNIA [1,2] (Fellow, IEEE), AND ROBERTA PALMERI [1,2] (Member, IEEE)

[1]Dipartimento di Ingegneria dell'Informazione, delle Infrastrutture e dell'Energia Sostenibile, Università Mediterranea of Reggio Calabria, 89124 Reggio Calabria, Italy
[2]Istituto per il Rilevamento Elettromagnetico dell'Ambiente, Consiglio Nazionale delle Ricerche, 80124 Naples, Italy

CORRESPONDING AUTHOR: R. PALMERI (e-mail: roberta.palmeri@unirc.it).

This work was supported in part by the Italian National Recovery and Resilience Plan (NRRP) of NextGenerationEU, partnership on "Telecommunications of the Future" under Grant PE00000001 - program RESTART; in part by the Italian Ministry of University and Research with projects "IDEAS - Inverse Design of terahertz interAction Structures" under Grant PRIN2022 PNRR P202293B5X; and in part by the "MEETAPP – MEtasurface-based tEchnology Towards industrial APPlications" under Grant PRIN2022 P2022ZZ8APA.

ABSTRACT Electromagnetic scattering from a set of scatterers located above a planar perfect electric conductor is a canonical problem that is relevant to many scenarios of practical interest. In this work, we focus on the canonical case of arbitrarily shaped cylinders with parallel axes, which is of interest for the analysis and synthesis of metagratings and reconfigurable intelligent surfaces. This scenario is also pivotal for synthesizing such structures through inverse design approaches. In particular, a simple and effective strategy for analyzing the scattering behavior of this kind of structures is proposed. The developed tool is compared with commercial simulation software, showing its ability to provide comparable results with significantly higher computational efficiency.

INDEX TERMS Inverse design, metagratings, metasurfaces, mutual scattering, scattering matrix, scattering problems.

I. INTRODUCTION

THE evaluation of the electromagnetic (EM) scattering from a set of distinct objects in a given environment is a very relevant problem, as witnessed from the large number of related applications [1], [2], [3], [4], [5], [6], [7], [8], [9], [10], [11], [12], [13], [14], [15], [16], [17], [18], [19], [20], [21], [22], [23]. These include radar systems, EM compatibility, molecular scattering [4], [5] composite materials, and innovative artificial materials-based devices [23], [24], [25]. In fact, accurate analysis and design of scattering behavior (through the proper location and choice of the scatterers) along with the appropriate design of primary sources represents the only available ways to shape the EM field to meet specific application requirements.

Recent examples in ICT applications include the design of devices such as reconfigurable intelligent surfaces (RIS) [26], [27], [28], metagratings [24], [25], [29], arrays and reflectarrays [30], [31], metasurfaces [32], invisibility cloaks [33], and smart skins [34]. Notably, in these applications it is often required to solve the scattering problem in the presence of a planar perfect electric conductor (PEC). Accordingly, in the following, we focus on the canonical case of 2D parallel cylinders with arbitrary cross-section in the presence of a PEC plane.

In the literature, several contributions address the 2D scattering from cylinders with arbitrary cross-section in free space (see [1], [10], [11], [12], [18], [23] and references therein), as well as in the presence of a planar infinite discontinuity (e.g., PEC) [2], [3], [6], [7], [8], [9], [13], [14], [15], [16], [17], [19], [20], [21], [22]. However, the referenced works handle the problem through approaches that differ completely from the one proposed in this paper. Typically, they focus on a single or very limited number of scatterers [1], [2], [6], [20], which are also small compared to the wavelength. As a result, the scatterers are approximated to wires, allowing for straightforward application

of the image theory and/or first-order approximations of the scattering problem. Other works instead rely on full-wave analysis and numerical methods [17], which makes the solution process computationally heavy, or are specifically derived for canonical shapes [3], [10], [13], [14], [15], [16]. Finally, another set of approaches focuses on periodic arrangements of scatterers [24], [25], thereby missing many practical scenarios and losing possible degrees of freedom available in the corresponding synthesis problems.

In contrast, our approach allows handling many (and potentially different) scatterers and enables a more comprehensive evaluation of both their individual scattering contributions and the cooperative effects among them.

To this end, we show in the following how the problem can be conveniently solved in the framework of the so-called scattering matrix method (SMM), originally developed in [11] for scattering in free space and more recently adopted for the design of graded metamaterials-based antennas and guiding devices [35], [36], [37].

The SMM is based on representing the electromagnetic properties and response of each scatterer using a scattering matrix (as defined in [11]), which relates the coefficients of a suitable representation basis for the incident and scattered fields. In this way, the scattering problem is reduced to a system of linear equations, where the known terms encode the primary incident field (e.g., the field generated by the primary source in the absence of the obstacles), while the unknowns are the coefficients of the field scattered by each cylinder.

Notably, as stated in the original paper of Felbacq [11], although other authors (e.g., [10]) had used a similar formalism for the specific case of circular cylinders, the concept of the scattering matrix allows for a generalization to arbitrarily shaped cylinders without introducing a computational overhead (but for simple preliminary offline computations).

The ability to consider (and quickly analyze) this kind of scenarios considerably extends the range of cases that can be addressed using the analytical tools presented in [24], [25] and related references. Obviously, many tools can be employed to analyze the scattering phenomenon under consideration, ranging from full-wave numerical procedures that discretize the volume under test into pixels (or voxels) to homogenization theory. Actually, full-wave simulations provide high accuracy, but come with drawbacks in terms of computational burden and, hence, scalability. On the other hand, homogenization procedures overcome this limitation but are intrinsically approximate, as they hold for sufficiently smooth varying objects. In this respect, scatterers-oriented tools (such as the SMM) represent a suitable alternative at a *mesoscale* level. In fact, while still guaranteeing high accuracy, they considerably reduce the number of unknowns with respect to general purpose numerical simulators and do not rely on local-periodicity assumptions.

Last but not least, thanks to the above-mentioned features, the developed model can be readily applied within an inverse design framework, as successfully demonstrated by some of the authors in the free-space case [36], [37]. This paves the way for the efficient and controlled design of devices such as RIS, metagratings and similar technologies.

With respect to the problem dealt with in this work, i.e., the scattering from N arbitrary shaped cylinders in presence of a PEC plane, the proposed SMM-based approach exploits the simple yet effective idea of introducing *image* scatterers whose scattered fields are such to satisfy the boundary conditions at the PEC surface. Notably, the presence of the PEC and the position of the scatterers with respect to it are properly accounted for in the final system. This allows to formulate the overall scattering problem by still using the free-space scattering matrix of each scatterer, resulting in a remarkable conceptual simplification and a benefit in terms of computational burden.

The paper is organized as follow. Section II is devoted to deriving a proper representation of the field scattered by arbitrary cylindrical objects positioned above a planar PEC surface, for both E-parallel and H-parallel field polarization. Section III presents the formulation of the proposed Combined Image Theory Scattering Matrix Method (CIT-SMM) for fast and effective analysis of the forward scattering problem at hand. The aim of Section IV is to evaluate the accuracy and computational efficiency of the developed approach and associated codes, while in Section V the CIT-SMM is applied to more applicative scenarios. Conclusions are drawn in Section VI. Finally, three Appendices provide further details on specific implementation aspects.

A 2D scalar formulation of the problem is considered for both field polarizations, and the adopted time dependence is of the form $e^{j\omega t}$.

II. FIELDS REPRESENTATION IN CASE OF CYLINDERS ABOVE A PLANAR PEC

The interaction of the incident field with scatterers having specific EM features modifies the original (incident) field, resulting in the so-called scattered field. Moreover, the presence of the PEC plane further alters the overall scattering phenomenon with respect to the free-space scenario, leading to the challenge of computing the resulting field in an efficient manner.

In this contribution, we take advantage of the planar nature of the PEC to derive the total scattered field in the upper half-space by extending the concept of *image sources* to non-wire-like scatterers. In this approach, the PEC plane is considered as an additional scatterer whose response is computed as the superposition of two contributions: the first corresponds to the reflection of the incident field from the PEC when no scatterer is present, and the second arises from the fields radiated by *image* scatterers located behind the plane.

The scattering problem at hand is sketched in Fig. 1(a), where a finite number N of arbitrarily shaped scatterers, parallel to the z-direction and invariant along it, are positioned in front of an infinite planar PEC surface parallel to the

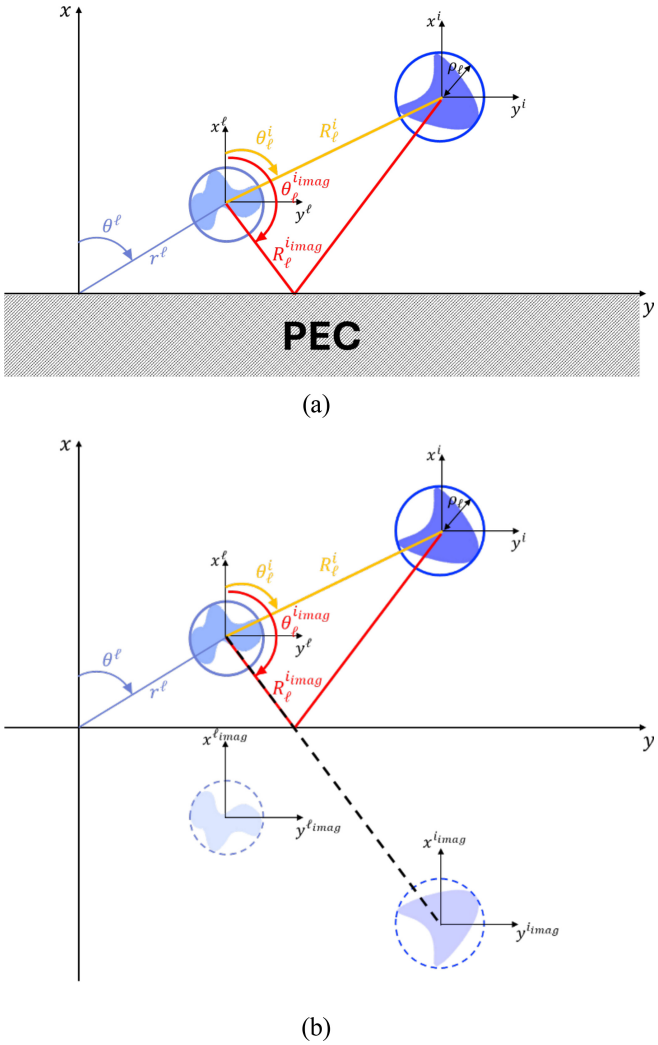

FIGURE 1. (a) Original scattering scenario involving cylinders in the presence of an infinite planar PEC. (b) Equivalent free-space scenario obtained by modeling the scattering phenomenon in (a) through the *image* principle.

y-axis. In contrast, Fig. 1(b) shows the equivalent scenario in which the PEC is substituted by proper *image* scatterers.

In the following, Section II-A and II-B will focus, respectively, on the E-polarization and H-polarization case, where it is understood that the field (E or H) is parallel to both the cylinders axis (i.e., the z-axis) and the planar PEC surface.

A. E-POLARIZATION

Let us consider a cylindrical harmonics expansion[1] of the incident (as generated by the primary source) electric field on the ℓ-th cylinder, i.e.,:

$$E_{inc_\ell} = \sum_{m=-\infty}^{\infty} Q_{\ell,m} J_m(k_0 R_\ell) e^{jm\theta_\ell} \tag{1}$$

In this latter, J_m is the m-th order Bessel function, k_0 is the free-space wavenumber and (R_ℓ, θ_ℓ) denotes an arbitrary point in the space of coordinates (x, y), defined with respect to the local reference system of the ℓ-th scatterer.

By using the same modal expansion, the electric field scattered by the actual ℓ-th cylinder as if it were in free-space can be represented as:

$$E^{actual}_{scat_\ell} = \sum_{m=-\infty}^{\infty} b^E_{\ell,m} H^{(2)}_m(k_0 R_\ell) e^{jm\theta_\ell} \tag{2}$$

where $H^{(2)}_m$ is the m-th order Hankel function of second kind.

Based on the above considerations regarding the applicability of the image theory, the overall scattered electric field for the inhomogeneous scenario at hand, due to the ℓ-th cylinder, can be computed as:

$$E_{scat_\ell} = E^{actual}_{scat_\ell} + E^{image}_{scat_\ell} + E^{PEC}_{scat_\ell} \tag{3}$$

$E^{PEC}_{scat_\ell}$ and $E^{image}_{scat_\ell}$ being, respectively, the reflection from the PEC plane of the primary incident field and the field scattered by the ℓ-th *image* cylinder.

In formulas:

$$E^{PEC}_{scat_\ell} = E^{refl}_{inc_\ell} = \sum_{n=-\infty}^{\infty} Q'_{\ell,n} J_n\left(k_0 R'_\ell\right) e^{jn\theta'_\ell} \tag{4}$$

$$E^{image}_{scat_\ell} = \sum_{n=-\infty}^{\infty} b^{E'}_{\ell,n} H^{(2)}_n\left(k_0 R'_\ell\right) e^{jn\theta'_\ell} \tag{5}$$

where in (R'_ℓ, θ'_ℓ) indicates an arbitrary point in the reference system of the ℓ-th *image* scatterer.

Finally, once each ℓ-th field is expressed in a unique reference system, the overall scattered field is given by summing (3) over the total number N of cylinders.

Notably, the expansion coefficients $Q_{\ell,m}$ in (1) and $Q'_{\ell,n}$ in (4) can be easily computed based on the kind of primary source (see Appendix A).

Since the PEC plane is present, the tangential component of the overall scattered electric field must be cancelled out at x=0. This condition implies that the coefficients $b^{E'}_{\ell,n}$ are dependent on the coefficients $b^{E}_{\ell,m}$ (or vice versa). As a consequence, the overall contribution from both the actual cylinders and their *images* can be expressed solely in terms of the coefficients $b^{E}_{\ell,m}$.

Notably, the nulling of the tangential electric fields can be enforced for each 'actual+image' scatterer pair individually, without considering the summation over all cylinders. In fact, since both uniqueness and linearity hold true [40], once a solution is found for each pair, the solution built by the superposition of effects becomes the unique solution, as it satisfies both the boundary conditions and the Sommerfeld radiation condition at infinity.

Accordingly, the condition to enforce for each pair is the following:

$$\sum_{m=-\infty}^{\infty} b^E_m H^{(2)}_m(k_0 R_\ell) e^{jm\theta_\ell} = -\sum_{n=-\infty}^{\infty} b^{E'}_n H^{(2)}_n(k_0 R_\ell) e^{jn\pi} e^{-jn\theta_\ell} \tag{6}$$

[1]Notably, other choices are also possible [38], [39].

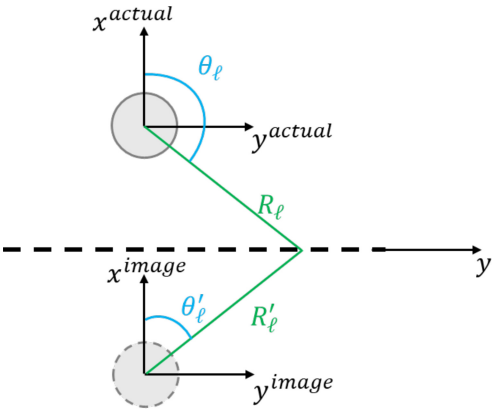

FIGURE 2. Detail of the reference system for the actual scatterer and its corresponding *image*.

where the relations $R'_\ell = R_\ell$ and $\theta'_\ell = \pi - \theta_\ell$ have been used, see Fig. 2. Then, by considering the substitution $n = -m$ and using the property of the Hankel function $H^{(2)}_{-m}(z) = (-1)^m H^{(2)}_m(z)$, one gets that, in the chosen reference system, eq. (6) is satisfied $\forall \ell$ if:

$$b^{E'}_m = -b^E_{-m} \tag{7}$$

Notably, as the actual coefficients in (2) and (5) depend on the chosen reference system, eq. (7) holds true for the case where the reference axes for the polar system on the cylinders are perpendicular to the planar PEC. Other relationships amongst the set of primed and unprimed coefficients [which can be easily inferred by processing (6) and (7)] will hence hold true for different choices of the polar reference system.

B. H-POLARIZATION

In the case of H-polarization, the formalism presented in Section II-A can still be applied, but with reference to the magnetic field. The corresponding electric fields can then be computed by directly applying Maxwell's equations.

Both the incident and reflected magnetic field for the ℓ-th actual and *image* cylinder can be expressed in terms of cylindrical harmonics as:

$$H_{inc_\ell} = \sum_{m=-\infty}^{\infty} Q_{\ell m} J_m(k_0 R_\ell) e^{jm\theta_\ell} \tag{8}$$

$$H^{PEC}_{scat_\ell} = H^{refl}_{inc_\ell} = \sum_{n=-\infty}^{\infty} Q'_{\ell,n} J_n\left(k_0 R'_\ell\right) e^{jn\theta'_\ell} \tag{9}$$

where the coefficients $Q_{\ell,m}$ and $Q'_{\ell,n}$ can still be computed based on the type of primary source (see Appendix A).

The same arguments apply to the scattered magnetic fields that read:

$$H^{actual}_{scat_\ell} = \sum_{m=-\infty}^{\infty} b^H_{\ell,m} H^{(2)}_m(k_0 R_\ell) e^{jm\theta_\ell} \tag{10}$$

$$H^{image}_{scat_\ell} = \sum_{n=-\infty}^{\infty} b^{H'}_{\ell,n} H^{(2)}_n\left(k_0 R'_\ell\right) e^{jn\theta'_\ell} \tag{11}$$

Thus, the overall scattered magnetic field for the inhomogeneous scenario at hand, due to the ℓ-th cylinder, can be computed as:

$$H_{scat_\ell} = H^{actual}_{scat_\ell} + H^{image}_{scat_\ell} + H^{PEC}_{scat_\ell} \tag{12}$$

Since the overall tangential magnetic field has to double with respect to the incident one, the boundary condition on the PEC plane becomes:

$$\widehat{i}_n \times \left(H_{inc} + H^{actual}_{scat}\right)\widehat{i}_z\Big|_{PEC} = \widehat{i}_n \times \left(H^{refl}_{inc} + H^{image}_{scat}\right)\widehat{i}_z\Big|_{PEC} \tag{13}$$

where $\widehat{i}_n$ is the normal unit vector to the PEC plane, and the summation over the N cylinders is considered.

Notably, H^{refl}_{inc} can be easily computed to satisfy the boundary conditions on the PEC plane by using proper $Q'_{\ell,n}$ coefficients (see also Appendix A).

Conversely, to satisfy condition (13) for the scattered fields, a relationship amongst the coefficients $b^{H'}_{\ell,n}$ and $b^H_{\ell,m}$ of the representations must be derived.

By extending the same arguments given for the E-polarization case, this relationship can be derived by considering each actual+image pair individually. Therefore, $\forall \ell$:

$$\sum_{m=-\infty}^{\infty} b^H_m H^{(2)}_m(k_0 R_\ell) e^{jm\theta_\ell} = \sum_{n=-\infty}^{\infty} b^{H'}_n H^{(2)}_n(k_0 R_\ell) e^{jn\pi} e^{-jn\theta_\ell}, \tag{14}$$

where the relations $R'_\ell = R_\ell$ and $\theta'_\ell = \pi - \theta_\ell$ have been used. Again, by considering the substitution $n = -m$ and the above cited property of Hankel functions, it follows that in the chosen reference system (see Fig. 2) eq. (14) holds $\forall \ell$ if:

$$b^{H'}_m = b^H_{-m}. \tag{15}$$

III. A COMBINED IMAGE THEORY SCATTERING MATRIX METHOD (CIT-SMM)

In the canonical free-space case, the idea underlying the SMM [11] is that the EM properties of a given target can be encoded in the so-called scattering matrix. This matrix relates the coefficients of the representation bases of the incident and scattered field as follows:

$$\mathbf{b}_\ell = \mathbf{S}_\ell \mathbf{a}_\ell, \tag{16}$$

where, for the ℓ-th scatterer, $\mathbf{a}_\ell$ and $\mathbf{b}_\ell$ denote the vectors of coefficients corresponding to the incident and scattered field, respectively, while $\mathbf{S}_\ell$ is the scattering matrix whose expression is available in analytical form for canonical shapes [41] (whereas offline numerical simulations are required to determine it for non-canonical shapes).

Notably, the adoption of cylindrical harmonics expansions for both the incident and scattered fields facilitates accounting for the degrees of freedom of each scatterer, that is, the (finite and) minimal number of harmonics required to accurately represent any actual non-superdirective incident and scattered fields [42] (as reported in [43]), [44].

By so doing, the harmonics expansion can be truncated from $\lceil -k_0\rho_\ell \rceil$ to $\lceil k_0\rho_\ell \rceil$, where ρ_ℓ is the radius of the minimal circle enclosing the scatterer at hand, and symbol $\lceil . \rceil$ indicates the upper integer [44]. It follows that the overall number of unknowns grows with the sum of the perimeters of each cylinder, whereas standard numerical approaches would imply a number of unknowns growing with the sum of the scatterers' areas (when using the method of moments) or with the overall area of interest (when using other methods). Such a circumstance allows the proposed approach to achieve significant reductions in terms of computational burden.

Moving to the scenario addressed in this manuscript, it is worth noting that modeling the PEC plane as an additional scatterer justifies the adoption of the scattering matrix as defined for the free-space case, since the contribution of the plane is embedded through the *image* scatterers and their related scattering matrices.

Hence, by rewriting the harmonics field representations of Section II into a unique reference system through the Graf's addition theorem (see [11] for more details), the overall incident field (electric or magnetic, depending on the adopted polarization) on the ℓ-th scatterer can be expressed in matrix form through the vector of coefficients:

$$\mathbf{a}_\ell = \mathbf{Q}_\ell + \mathbf{Q}_\ell^{refl} + \sum_{i=1, i\neq\ell}^{N} \mathbf{T}_{\ell,i}\mathbf{b}_i + \sum_{i=1}^{N} \mathbf{W}_{\ell,i}\mathbf{b}_i, \quad (17)$$

where the first and second term encode the direct contributions (i.e., the primary incident field and its reflection from the PEC), while the last two terms pertain to the fields scattered by the actual and *image* cylinders, which act as secondary incident fields on the ℓ-th scatterer.

In (17), $\mathbf{Q}_\ell$ (and hence $\mathbf{Q}_\ell^{refl}$) depends on the specific primary incident field (see Appendix A for details of some cases of interest), while the two summations allow taking into account the contributions from the actual and *image* scatterers to the overall field impinging on the ℓ-th scatterer at hand. Notably the transformation matrices $\mathbf{T}_{\ell,i}$ and $\mathbf{W}_{\ell,i}$ allow expressing these contributions directly in terms of the coefficients $\mathbf{b}_i$. As such, these matrices consider the reciprocal locations of the actual and *image* cylinders and, in the case of $\mathbf{W}_{\ell,i}$, also reflect the coefficient relationships derived earlier in (7) and (15).

Going into details, from [11] one has:

$$T_{\ell,i,m,q} = e^{j(q-m)\theta_\ell^i} H_{m-q}^{(2)}\left(k_0 R_\ell^i\right). \quad (18)$$

where $(R_\ell^i, \theta_\ell^i)$ denote the polar coordinates of the i-th scatterer in the reference system of the ℓ-th scatterer (see yellow path and yellow angle in Fig. 1(b)).

By extending (18) and incorporating the relationships in (7) and (15), the elements of $\mathbf{W}_{\ell,i}$ matrix can be expressed as:

$$W_{\ell,i,m,q} = \begin{cases} -T'_{\ell,i,m,q}, & E-polarization \\ T'_{\ell,i,m,q}, & H-polarization \end{cases} \quad (19)$$

TABLE 1. Geometrical parameters of the cylinders used in the numerical analysis.

Scenario	Radius ρ	Permittivity ε_r	Position (x_ℓ, y_ℓ)
1 dielectric cylinder	$\lambda/12$	2	$(2\lambda/3,0)$
1 metallic cylinder	$\lambda/12$	-	$(2\lambda/3,0)$
2 dielectric cylinders	$\lambda/12$	2	$(\lambda/6, \lambda/3)$, $(\lambda/3,-\lambda/4)$

wherein $T'_{\ell,i,m,q}$ are the elements of the $\mathbf{T}'_{\ell,i}$ matrix, which plays a role analogous to $\mathbf{T}_{\ell,i}$, but applies to *image* scatterers. These matrices modify the expansion coefficients according to the different reference systems. Accordingly:

$$T'_{\ell,i,m,q} = e^{j(q-m)\theta_\ell^{i_{imag}}} H_{m-q}^{(2)}\left(k_0 R_\ell^{i_{imag}}\right), \quad (20)$$

where $(R_\ell^{i_{imag}}, \theta_\ell^{i_{imag}})$ are the polar coordinates of the i-th *image* cylinder relative to the ℓ-th actual cylinder (see red-dashed path and red angle in Fig. 1(b)).

Finally, by substituting (17) into (16), one has the following system of linear equations:

$$\mathbf{b}_\ell - \sum_{i=1, i\neq\ell}^{N} \mathbf{S}_\ell \mathbf{T}_{\ell,i}\mathbf{b}_i - \sum_{i=1}^{N} \mathbf{S}_\ell \mathbf{W}_{\ell,i}\mathbf{b}_i = \mathbf{S}_\ell\left(\mathbf{Q}_\ell + \mathbf{Q}_\ell^{refl}\right), \quad \forall\ \ell = 1, ..N \quad (21)$$

Once the system in (21) is solved for the $\mathbf{b}_\ell$ unknowns (see Appendix B for implementation details), the scattered fields can be computed using (2) and (5) for E-polarization, or (10) and (11) for H-polarization. Then, the overall scattered field at any point outside the scatterers is obtained by summing over all N terms in (3) for E-polarization or in (12) for H-polarization.

In summary, the joint consideration of suitable representations of scattered (both electric or magnetic) fields, the formulation of the image theory in terms of these representations, and the scattering matrix concept allow to formulate the overall problem in a compact and efficient form.

IV. NUMERICAL ANALYSIS

To assess the accuracy and the computational efficiency of the proposed method, we compare the results obtained with the CIT-SMM with those obtained by using the full-wave commercial electromagnetic software Comsol Multiphysics. In particular, scenarios involving both dielectric and metallic cylinders with circular and non-circular cross-sections are considered.

To model the 2D scenario in Comsol, an air-filled rectangular domain embedding the cylinders was used. Perfectly matching layers (PML) were added on all sides of the domain except on the conductive plane, where a PEC boundary condition was imposed. A plane wave excitation was used as background field. Several numerical tests were performed by varying the set of scatterers (e.g., material, position, number)

TABLE 2. Geometrical parameters of the cylinders used in the numerical analysis for the 12 cylinders case.

	Cylinder ℓ											
	1	2	3	4	5	6	7	8	9	10	11	12
x_ℓ/λ	0.98	0.63	0.69	1.28	0.38	1.38	1.07	1.28	0.99	0.46	0.64	0.45
y_ℓ/λ	0.56	1.07	-0.98	-0.56	-1.78	1.36	-1.73	0.30	1.84	0.43	-0.42	1.47
ρ_ℓ/λ	0.12	0.17	0.20	0.39	0.13	0.26	0.11	0.22	0.24	0.13	0.18	0.12
ε_r	2	2	-	2	-	-	-	-	-	2	-	2

TABLE 3. NMSE values for the numerical examples in Section IV.

Scenario	Incidence angle, α_{inc}			
	30°	45°	60°	90°
1 diel. cylinder	2.95E-5	7.81E-6	4.98E-6	3.62E-6
1 met. cylinder	2.76E-5	8.26E-6	4.63E-6	3.46E-6
2 diel. cylinders	3.03E-5	8.10E-6	5.2E-6	3.62E-6
12 mix. cylinders	1.00E-4	2.00E-4	1.00E-4	2.00E-4

TABLE 4. SSIM values for the numerical examples in Section IV.

Scenario	Incidence angle, α_{inc}			
	30°	45°	60°	90°
1 diel. cylinder	0.9949	0.9949	0.9951	0.9949
1 met. cylinder	0.9954	0.9951	0.9953	0.9954
2 diel. cylinders	0.9945	0.9943	0.9942	0.9942
12 mix. cylinders	0.9880	0.9873	0.9876	0.9880

as well as the direction of incidence of the plane wave. Geometrical details are reported in Tables 1 and 2.

For the sake of brevity, the computed scattered field is shown for just a single test case, while the results for all examples are compared using quantitative metrics summarized in Tables 3 and 4. In particular, the considered metrics are the normalized mean square error (NMSE)[2] between the Comsol-computed complex field, E_{scat}^{Comsol}, and the CIT-SMM result, $E_{scat}^{CIT-SMM}$, as well as the structural similarity index measure (SSIM) between the corresponding magnitude images. The metrics were evaluated over a $2\lambda\times4\lambda$ domain, except for the test case involving 12 cylinders, for which a $2.53\lambda\times5.6\lambda$ domain was considered. Concerning the truncation of fields representations, the dimensions of the involved scatterers led to consider 5 harmonics in all examples, except for the case with 12 mixed cylinders where 9 harmonics were used.

Finally, it is worth to underline that an advantage of the CIT-SMM lies in the fact that the **S** matrix for circular inclusions is diagonal and known in closed form for both dielectric and metallic cylinders [41].

[2]In our case, it is more appropriately described as a measure of discrepancy rather than an error.

Figure 3 shows the amplitude and phase of the scattered field for the case of N=12 randomly distributed cylinders with different radii and materials (see the first row of Figure 3 and Table 2 for details). Specifically, results obtained using the proposed method are compared with those derived from Comsol. A visual inspection of the field distribution within the domain, combined with the quantitative metrics, confirms that the developed tool provides highly accurate field evaluations in close agreement with Comsol results. This observation holds across all numerical test cases, as summarized in Tables 3 and 4.

To demonstrate the capability of the proposed technique to deal with non-circularly symmetric cylinders, we consider a case involving metallic strips. In particular, an alignment of 5 metallic strips, each of dimensions $0.1\lambda\times0.5\lambda$, is placed at a height of $2\lambda/3$ above the PEC plane, with a spacing of 0.75λ between strips. In order to apply the CIT-SMM to this scenario, the **S** matrix describing the free-space scattering behavior of a strip is needed. For non-circularly symmetric obstacle (where analytical expressions are generally unavailable) this matrix must be derived numerically using commercial solvers. Details of the procedure can be found in Appendix C.

The real and imaginary parts of the computed scattering matrix for the metallic strip involved in this example are shown in Fig. 4. Given the strip dimensions, the harmonics representation was truncated to the first 11 terms. Fig. 5 compares the scattered field computed using CIT-SMM (left column) with that obtained from Comsol (right column), again confirming the effectiveness and accuracy of the proposed approach. Note that, according to the analytical derivation, the CIT-SMM field representation is valid at all points outside the minimum circle enclosing each scatterer, that is, outside the regions bounded by dashed black lines in Fig. 5. Within the validity domain, the computed metrics are: NMSE=9.49E-5 and SSMI=0.9996.

As the Comsol simulations embed diffraction effects from edges, a larger computational domain ($90\ \lambda\times90\ \lambda$) was considered to ensure these effects become negligible, enabling a fair comparison with our results based on the hypothesis of an infinitely extended PEC plane.

Regarding computational costs, the overall simulation time using our method was only a few seconds in the worst case, while Comsol simulations (also considering the larger domain, see above) took several minutes. Notably, solving the system in (21) took only fractions of a second, with

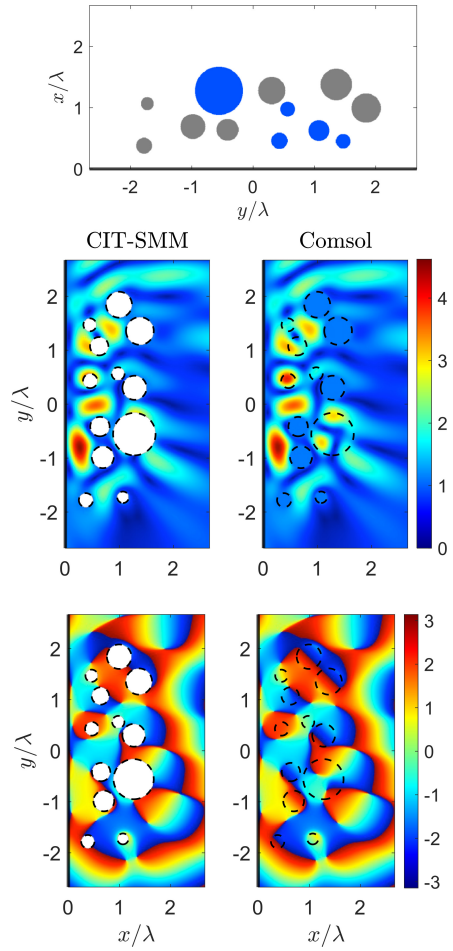

FIGURE 3. Scenario with 12 mixed cylinders. The first row shows the simulated configuration, where blue cylinders are dielectrics (e_r= 2) and gray cylinders are PEC. The second and third rows display the magnitude and phase, respectively, of the total scattered field, E_{scat}, computed using CIT-SMM (left column) and Comsol full-wave simulation (right column), for 45° incident plane wave.

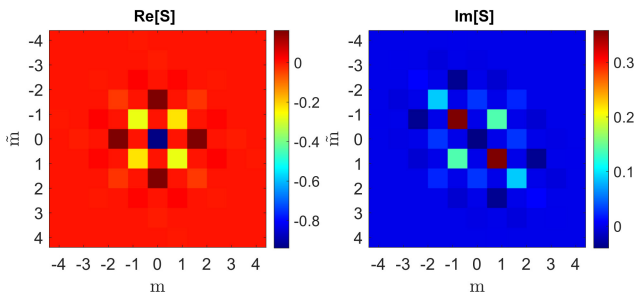

FIGURE 4. Numerical scattering matrix of a metallic strip with dimension $0.1\lambda \times 0.5\lambda$: real part (top) and imaginary part (bottom).

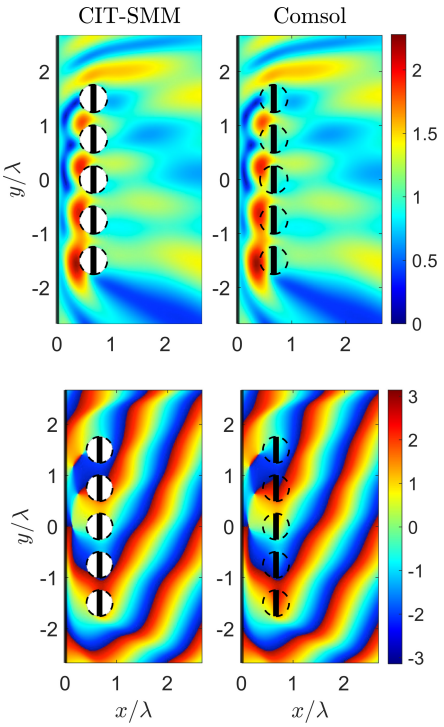

FIGURE 5. Five aligned metallic strips of size $0.1\lambda \times 0.5\lambda$, positioned $2\lambda/3$ above the PEC. Magnitude (left) and phase (right) of the total scattered field, E_{scat}, computed using CIT-SMM (left column) and Comsol full-wave simulation (right column), for 60° incident plane wave.

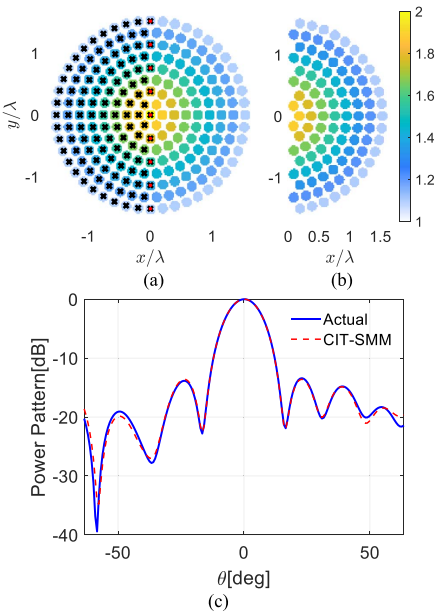

FIGURE 6. Luneburg lens example. (a) Dielectric distribution profile of the entire lens; (b) profile of the half lens. In (a), black cross markers indicate the rods replaced by the PEC in the half-lens configuration, while red dot markers indicate the rods lying along the symmetry plane, which do not have a corresponding *images*. (c) Power pattern distribution of the entire and half lenses.

the remaining computation time attributed to assembling the overall matrix ruling (21) and evaluating the field over the observation domain.

All simulations were performed on a workstation equipped with an Intel Xeon w5-2455X processor and 256 GB RAM.

V. CIT-SMM IN ACTUAL APPLICATIONS

To appraise the performance of the proposed approach in application-relevant scenarios, we simulated the behavior of a set of small inclusions properly organized to realize specific radiating functionalities.

As a first possibility, we considered a specific cylinders arrangement for the realization of artificial-materials-based lens antennas, a topic previously considered by the authors

also from an inverse design point of view [36], [37]. In this respect, let us note that, for the E-polarization, all the relationships described above can be directly applied to the case of cylinders in a parallel plate waveguide [45], enabling the design of a lens manipulating the field in a plane.

We leverage herein the property of a Luneburg lens, whereby its size can be halved by putting a PEC plane along the axis of symmetry, allowing field steering (over a halved range) without deformations [46], [47]. Accordingly, in order to both develop a reduced-size scanning antenna and compare its performance with the full lens, in the following we examine the case of a half Luneburg-like antenna realized by means of properly graded cylinders.

The relative dielectric permittivity distribution of a z-invariant canonical Luneburg lens is defined as:

$$\varepsilon_r(\underline{r}) = 2 - \underline{r}^2 \; for \; |\underline{r}| \leq 1. \tag{22}$$

Starting from this continuous distribution, we realize the corresponding discrete lens by sampling it according to a given arrangement of small circular scatterers. In our example, the lens is composed of N=217 fixed circular cylinders with radius λ/12 and having an overall radius equal to 1.5λ. The resulting device is depicted in Fig. 6(a). We then introduce a PEC plane along the vertical axis to serve as a symmetry plane. As a result, cylinders located in the region $x \leq 0$ [identified by crosses in Fig. 6(a)] are removed, yielding the configuration in Fig. 6(b).

Fig. 6(c) shows the power pattern radiated by the entire (blue continuous line) and halved (red dashed line) lens when a line-current positioned 0.4λ far from the lens's rim is used as primary feed. As it can be seen, the two patterns closely match, confirming that the half device performs congruently with the entire lens. Notably, this remains true even though the 9 cylinders located at $x = 0$ [touching the PEC surface, see red crosses in Fig. 6(a)] are completely neglected in the CIT-SMM, since their *images* cannot form.

As shown in [35], [36], similar results can be achieved by substituting dielectric cylinders having a varying permittivity with PEC cylinders of appropriately chosen variable radii (see [35] for more details).

Beyond this application, the findings validate the proposed approach for efficient analysis of symmetric structures and confirm the capability of the CIT-SMM to deal with line-current generated incident fields.

The second scenario is inspired by metagratings (structures composed of small objects above a planar PEC) [24], [25] that enable 'anomalous reflection', i.e., an overall scattered field focused on a direction not predicted by the Snell's law.

By leaving aside the complete and accurate inverse design of such a device (which is deferred to future work), we exploit the fact that the scattering matrix of circularly symmetric cylindrical objects is known in a closed form, along with the established requirement that, at a macroscopic level, a linear phase variation in the overall scattered field is needed [48], as measured just above the metagrating.

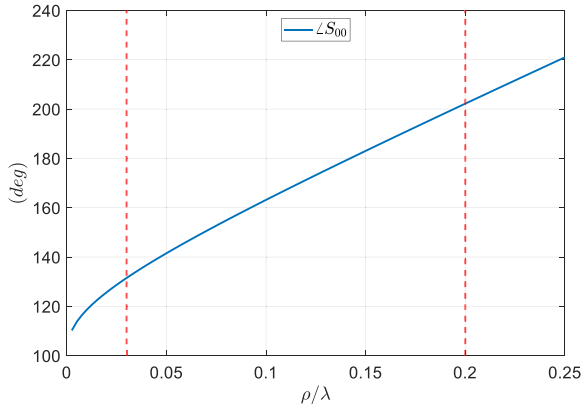

FIGURE 7. Phase of the m=0 order scattering coefficient as a function of the radius ρ of a metallic cylinder.

Hence, a first solution to the synthesis of a metagrating allowing anomalous reflection can be given under the hypothesis of small metallic cylinders, as follows: (i) choose the distance between each cylinder and the PEC plane to ensure positive interference between each scatterer and its *image* in the desired reflection direction; (ii) choose metallic cylinders radii to get a linear phase variation in the scattered field above the metagrating. Because the cylinders are small, the dominant scattering coefficient S_{00} governs the response. The analytically known phase behavior of S_{00} (see Fig. 7) shows an approximately linear variation with the cylinders dimensions in the evidenced [0.03-0.2]λ interval. As a consequence, by ignoring mutual coupling amongst cylinders, some (limited) phase control can be gained by adjusting cylinders radii accordingly.

Using this concept, we considered a linear array of $N = 9$ metallic circular cylinders illuminated by a plane wave coming from the direction orthogonal to the PEC plane. Based on the above arguments, in order to realize an anomalous reflection, we set the inter-cylinders spacing equal to λ/2, while the distance between cylinders and the plane was chosen approximately λ/4 to get a positive interference at 15°. Then, by exploiting the results in Fig. 7, the interval of ρ corresponding to a linear S_{00} phase was uniformly sampled into N=9 values assigned to the cylinders [see Fig. 8(a)].

Fig. 8(b) shows the resulting overall scattered field. Although having limited extent (neglecting higher-order harmonics and mutual coupling amongst cylinders), the design demonstrates an observable anomalous reflection phenomenon. More pronounced anomalous reflection is expected with scatterers offering greater S_{00} phase variability. In this respect, loaded or reconfigurable obstacles (such as those in [24], [25]) are expected to guarantee much more degrees of freedom.

In our understanding, the above results, combined with the CIT-SMM's ability to rapidly analyze structures with varying parameters, point to the method's potential as a powerful tool for the inverse design of metagratings and/or RIS inspired devices. In fact, one could properly engineer

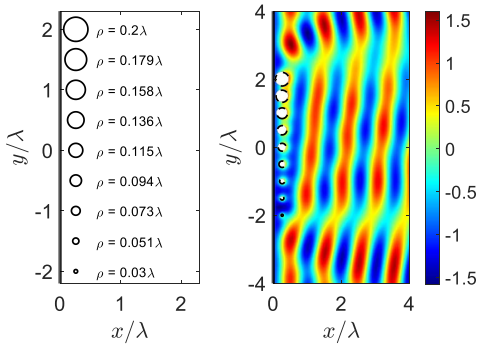

FIGURE 8. Metagratings-inspired device. Sketch of the alignment of metallic cylinders with varying dimensions (left). Real part of the total scattered field computed using CIT-SMM for a plane wave incident field normal to the PEC plane (right).

the structure, from both an electromagnetic and geometrical point of view, to realize anomalous/unconventional reflection of the impinging field, avoiding wire approximation of the cylinders and local periodicity assumptions. Ongoing work is focused on advancing these capabilities.

VI. CONCLUSION

A simple and effective approach for evaluating the scattered field (under both E-parallel and H-parallel polarizations) from a set of parallel cylinders in the presence of a planar and infinite perfect electric conductor has been proposed, developed and validated. The method leverages the image theory (as particularized in terms of the representations of the different scattered fields), and the scattering matrix concept [11], which relates the coefficients of a proper expansion basis for the incident and scattered field.

This approach enables encoding the electromagnetic properties of the scatterers within their scattering matrices as defined for the free space case, while mutual interactions are incorporated into the matrix coefficients of the resulting linear system. Solving this system provides the total scattered field.

The proposed tool has been successfully validated through comparison with full-wave simulations and applied to scenarios of interest for ICT. Notably, the use of the scattering matrix concept allows for generalization to arbitrary-shaped cylinders without additional computational overhead (but for simple, preliminary offline computations), thus broadening the applicability of the proposed tool. To the best of our knowledge, despite its conceptual simplicity, this kind of approach has not been systematically considered in the literature.

Furthermore, the availability of closed-form expressions for the scattering matrix coefficients of canonical objects enables the realization of unconventional functionalities. As demonstrated in our prior work on free-space scatterers [35], [36], [37], such an analysis tool can be profitably employed in the optimal inverse design of devices, such as reconfigurable intelligent surfaces, metagratings, and metaprisms, without relying on global optimization algorithms.

While the final goal of our investigation includes the development of such inverse design capabilities and the extension of the tool to 3D scenarios, these aspects fall outside the scope of the present contribution.

APPENDIX A
DETAILS ON THE COMPUTATION OF THE ELEMENTS OF THE Q VECTOR

It is worth to consider that, whatever the adopted polarization, any incident field can be expressed as a superposition of cylindrical harmonics. For example, in the case of line sources, the incident field can be expressed using the fundamental harmonics in its natural reference system, and then expanded into the local harmonics of any given cylinder by means of the Graf's addition theorem [49].

Ultimately, in all cases, the different sources simply modify the entries of the $\mathbf{Q}$ matrix in the final linear system of equations (21) in a known fashion.

For the case of an incident field generated by either a plane wave or a line source, the following analytical expression hold [11], [36]:

$$Q_{\ell,m} = \begin{cases} e^{-jk_0 r^\ell \sin(\alpha_{inc}-\theta^\ell)} e^{-jm\alpha_{inc}} & plane\ wave\ (pw) \\ -\frac{\omega\mu_0 I_s}{4} H_m^{(2)}\left(k_0 r_{ls}^\ell\right) e^{-jm\theta_{ls}^\ell} & line\ source\ (ls) \end{cases} \tag{A.1}$$

where α_{inc} is the incidence angle with respect to the y-axis, I_s indicates the intensity of the line source, and $(r_{ls}^\ell, \theta_{ls}^\ell)$ are its polar coordinates with respect to the ℓ-th cylinder's reference system, see Fig. 9 for notation.

Accordingly, for the considered reference system with the PEC plane parallel to the y-axis, one gets:

$$Q_{\ell,m}^{refl} = \begin{cases} \mp e^{jk_0 r^\ell \sin\left(\alpha_{inc}^{imag} - \theta^{\ell^{imag}}\right)} e^{-jm\alpha_{inc}^{imag}} & pw \\ \pm \frac{\omega\mu_0 I_s}{4} H_m^{(2)}\left(k_0 r_{ls}^{\ell^{imag}}\right) e^{-jm\theta_{ls}^{\ell^{imag}}} & ls \end{cases} \tag{A.2}$$

with $(r_{ls}^{\ell^{imag}}, \theta_{ls}^{\ell^{imag}})$ being the coordinate of the *image* line source with respect to the ℓ-th reference system. The sign depends on the field polarization: the upper sign corresponds to E-parallel polarization, and the lower sign to H-parallel polarization.

APPENDIX B
CIT-SMM IMPLEMENTATION DETAILS

Following [11], eq. (21) can be written in matrix form as:

$$\left[[\mathbf{A}] + \left[\mathbf{A}'\right]\right][\mathbf{b}] = [\mathbf{S}]\left[[\mathbf{Q}] + \left[\mathbf{Q}'\right]\right], \tag{A.3}$$

This represents a linear system of equations, where $\mathbf{b}$ is the column vector of unknown scattered field coefficients, b_m, and $\mathbf{Q}$ and $\mathbf{Q}'$ are the column vectors representing the incident and reflected field coefficients, respectively. $\mathbf{S}$ is the scattering matrix.

Let us focus on matrices $\mathbf{A}$ and $\mathbf{A}'$. By denoting $\mathbf{I}$ as the unit matrix, and following [11], the matrix $\mathbf{A}$, associated with the actual cylinders, is given by:

$$\mathbf{A} = \begin{bmatrix} \mathbf{I} & -\mathbf{S_1T_{1,2}} & \dots & -\mathbf{S_1T_{1,N}} \\ -\mathbf{S_2T_{2,1}} & \mathbf{I} & \dots & -\mathbf{S_2T_{2,N}} \\ \vdots & \dots & \ddots & \vdots \\ -\mathbf{S_NT_{N,1}} & -\mathbf{S_NT_{N,2}} & \dots & \mathbf{I} \end{bmatrix}. \quad \text{(A.4)}$$

The detailed formulation of the submatrices in $\mathbf{A}$ is reported in (A.5), shown at the bottom of the page.

The matrix $\mathbf{A}'$, corresponding to the contributions from image cylinders, is given by:

$$\mathbf{A}' = \begin{bmatrix} -\mathbf{S_1W_{1,1}} & -\mathbf{S_1W_{1,2}} & \dots & -\mathbf{S_1W_{1,N}} \\ -\mathbf{S_2W_{2,1}} & -\mathbf{S_2W_{2,2}} & \dots & -\mathbf{S_2W_{2,N}} \\ \vdots & \dots & \ddots & \vdots \\ -\mathbf{S_NW_{N,1}} & -\mathbf{S_NW_{N,2}} & \dots & -\mathbf{S_NW_{N,N}} \end{bmatrix} \quad \text{(A.6)}$$

The detailed formulation of the submatrices in $\mathbf{A}'$ is reported in (A.7), shown at the bottom of the page.

Notably, $\mathbf{A}'$ differs from $\mathbf{A}$ in two main aspects. First, $\mathbf{A}'$ does not contain unit matrices along the diagonal, as it accounts for the self-interaction of each cylinder with its own *image*.

Second, the submatrices $\mathbf{W}_{m,q}$ are horizontally flipped according to the conditions (7) or (15), depending on whether E-polarization or H-polarization is considered.

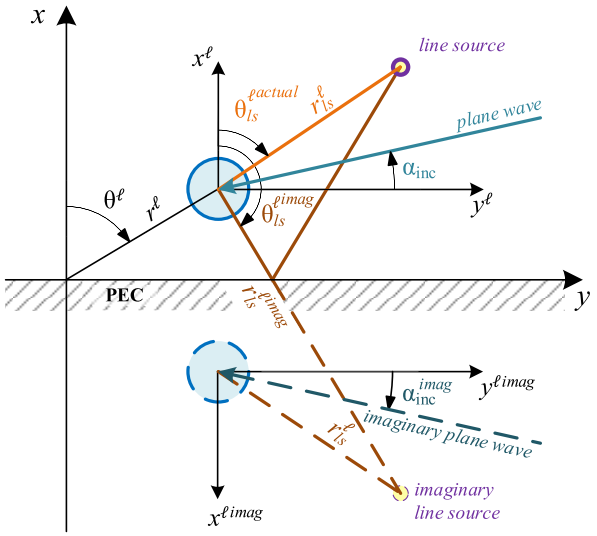

FIGURE 9. Notation adopted for the definition of line source and plane wave incident field.

The final system of equations for the multiple scattering problem involving cylinders in presence of a planar PEC is reported in (A.8) shown at the bottom of the page.

It is important to note that the matrices and vectors are truncated such that the harmonics indices m and q range from $-M$ to M, where $M = \lceil k_0\rho_\ell \rceil$

$$\mathbf{A} = \begin{bmatrix} \begin{bmatrix} 1 & 0 & \dots \\ 0 & 1 & 0 \\ \vdots & 0 & \dots \end{bmatrix} & -\begin{bmatrix} S_{1_{-M}}T_{1,2,-M,-M} & \dots & S_{1_{-M}}T_{1,2,-M,M} \\ \vdots & \ddots & \vdots \\ S_{1_M}T_{1,2,M,-M} & \dots & S_{1_M}T_{1,2,M,M} \end{bmatrix} & \dots \\ -\begin{bmatrix} S_{2_{-M}}T_{2,1,-M,-M} & \dots & S_{2_{-M}}T_{2,1,-M,M} \\ \vdots & \ddots & \vdots \\ S_{2_M}T_{2,1,M,-M} & \dots & S_{2_M}T_{2,1,M,M} \end{bmatrix} & \begin{bmatrix} 1 & 0 & \dots \\ 0 & 1 & 0 \\ \vdots & 0 & \dots \end{bmatrix} & \vdots \\ \vdots & \dots & \ddots \end{bmatrix} \quad \text{(A.5)}$$

$$\mathbf{A}' = \begin{bmatrix} -\begin{bmatrix} S_{1_{-M}}W_{1,1,M,M} & \dots & S_{1_{-M}}W_{1,1,M,-M} \\ \vdots & \ddots & \vdots \\ S_{1_M}W_{1,1,-M,M} & \dots & S_{1_M}W_{1,1,-M,-M} \end{bmatrix} & -\begin{bmatrix} S_{1_{-M}}W_{1,2,M,M} & \dots & S_{1_{-M}}W_{1,2,M,M} \\ \vdots & \ddots & \vdots \\ S_{1_M}W_{1,2,-M,M} & \dots & S_{1_M}W_{1,2,-M,-M} \end{bmatrix} & \dots \\ -\begin{bmatrix} S_{2_{-M}}W_{2,1,M,M} & \dots & S_{2_{-M}}W_{2,1,M,-M} \\ \vdots & \ddots & \vdots \\ S_{2_M}W_{2,1,-M,M} & \dots & S_{2_M}W_{2,1,-M,-M} \end{bmatrix} & \begin{bmatrix} S_{2_{-M}}W_{2,2,M,M} & \dots & S_{2_{-M}}W_{2,2,M,-M} \\ \vdots & \ddots & \vdots \\ S_{2_M}W_{2,2,-M,M} & \dots & S_{2_M}W_{2,2,-M,-M} \end{bmatrix} & \vdots \\ \vdots & \dots & \ddots \end{bmatrix} \quad \text{(A.7)}$$

$$\begin{bmatrix} \mathbf{I} - \mathbf{S_1W_{1,1}} & -\mathbf{S_1}(\mathbf{T_{1,2}} + \mathbf{W_{1,2}}) & \dots & -\mathbf{S_1}(\mathbf{T_{1,N}} + \mathbf{W_{1,N}}) \\ -\mathbf{S_2}(\mathbf{T_{2,1}} + \mathbf{W_{2,1}}) & \mathbf{I} - \mathbf{S_2W_{2,2}} & \dots & -\mathbf{S_2}(\mathbf{T_{2,N}} + \mathbf{W_{2,N}}) \\ \vdots & \dots & \ddots & \vdots \\ -\mathbf{S_N}(\mathbf{T_{N,1}} + \mathbf{W_{N,1}}) & -\mathbf{S_N}(\mathbf{T_{N,2}} + \mathbf{W_{N,2}}) & \dots & \mathbf{I} - \mathbf{S_NW_{N,N}} \end{bmatrix} \begin{bmatrix} \mathbf{b_1} \\ \mathbf{b_2} \\ \vdots \\ \mathbf{b_N} \end{bmatrix} = \begin{bmatrix} \mathbf{S_1}\left(\mathbf{Q_1} + \mathbf{Q_1^{refl}}\right) \\ \mathbf{S_2}\left(\mathbf{Q_2} + \mathbf{Q_2^{refl}}\right) \\ \vdots \\ \mathbf{S_N}\left(\mathbf{Q_N} + \mathbf{Q_N^{refl}}\right) \end{bmatrix} \quad \text{(A.8)}$$

Accordingly, the total size of matrices $\mathbf{A}$ and $\mathbf{A}'$ to be inverted for solving the system and evaluating the field coefficients is $(2M+1)N$.

APPENDIX C
DERIVATION OF THE SCATTERING MATRIX FOR NON-CANONICAL SHAPE OBJECTS

The numerical evaluation of the entries of the scattering matrix for non-canonical targets can be pursued through the following steps:

1) build a numerical model for the target at hand in free-space;
2) calculate the truncation index for the incident field harmonics representation as $M = \lceil k_0\rho \rceil$, where ρ is the radius of the smallest circle enclosing the scatterer [44]. Accordingly, the representations of the incident field [(1) for the E-polarization and (8) for the H-polarization] read:

$$\psi_{inc}(\underline{r}) = \sum_{m=-M}^{M} a_m J_m(k_0 r) e^{jm\theta} \tag{A.9}$$

ψ being the E or H longitudinal field component, parallel to the target's axis, depending on the considered case;
3) $\forall m$ and for unitary amplitude (that is, $a_m = 1$), solve the scattering problem for the numerical model by using $\psi_{inc}^{(m)}$ as incident field. Store the m-th computed scattered field as $\psi_{scat}^{(m)}$;
4) using the harmonics representation of the scattered field (eq. (2) or (10), properly truncated to $M = \widetilde{M}$), determine the representation coefficients $b_{\widetilde{m}}$ by solving the following least-squares minimization problem:

$$\min_{b_{\widetilde{m}}} \gamma^{(m)} \left\| \psi_{scat}^{(m)} - \sum_{\widetilde{m}=-\widetilde{M}}^{\widetilde{M}} b_{\widetilde{m}} H_{\widetilde{m}}^{(2)}(k_0 r) e^{j\widetilde{m}\theta} \right\|^2, \tag{A.10}$$

where $\gamma^{(m)}$ is a weighting factor equal to the inverse of the energy of $\psi_{scat}^{(m)}$. Note (A.10) must be performed at points outside the scatterer to avoid singularity issues.
5) By virtue of (15), since unitary harmonics were considered for the incident field, the retrieved $b_{\widetilde{m}}$ coefficients exactly correspond to the m-th column of the scattering matrix.

REFERENCES

[1] V. Twersky, "Multiple scattering of radiation by an arbitrary planar configuration of parallel cylinders and by two parallel cylinders," *J. Appl. Phys.*, vol. 23, no. 4, pp. 407–414, 1952.
[2] J. R. Wait, "Reflection from a wire grid parallel to a conducting plane," *Can. J. Phys.*, vol. 32, no. 9, pp. 571–579, 1954.
[3] K. Tabata and S. Kozakis, "Electromagnetic scattering by a conducting cylinder located near the conducting plane," *Electr. Commun. Japanese (Part-I, Commun.)*, vol. 63, no. 9, pp. 72–80, 1980.
[4] F. Borghese, P. Denti, R. Saija, G. Toscano, and O. I. Sindoni, "Multiple electromagnetic scattering from a cluster of spheres. I. Theory," *Aerosol Sci. Tech.*, vol. 3, no. 2, pp. 227–235, 1984.
[5] O. I. Sindoni, F. Borghese, P. Denti, R. Saija, and G. Toscano, "Multiple electromagnetic scattering from a cluster of spheres. II. Symmetrization," *Aerosol Sci. Tech.*, vol. 3, no. 2, pp. 237–243, 1984.
[6] E. Arvas, R. Harrington, and J. Mautz, "Radiation and scattering from electrically small conducting bodies of arbitrary shape above an infinite ground plane," *IEEE Trans. Antennas Propag.*, vol. 35, no. 4, pp. 378–383, Apr. 1987.
[7] T. C. Rao and R. Barakat, "Plane-wave scattering by a conducting cylinder partially buried in a ground plane. 1. TM case," *J. Opt. Soc. Amer. A* vol. 6, no. 9, pp. 1270–1280, 1989.
[8] T. C. Rao and R. Barakat, "Plane-wave scattering by a conducting cylinder partially buried in a ground plane II: TE case," *J. Opt. Soc. Amer. A* vol. 8, no. 12, pp. 1986–1990, 1991.
[9] G. Videen, "Light scattering from a sphere on or near a surface," *J. Opt. Soc. Amer. A*, vol. 8, no. 3, pp. 483–489, 1991.
[10] A. Z. Elsherbeni and A. A. Kishk, "Modeling of cylindrical objects by circular dielectric and conducting cylinders," *IEEE Trans. Antennas Propag.*, vol. 40, no. 1, pp. 96–99, Jan. 1992.
[11] D. Felbacq, G. Tayeb, and D. Maystre, "Scattering by a random set of parallel cylinders," *J. Opt. Soc. Amer. A*, vol. 11, no. 9, pp. 2526–2538, 1994.
[12] F. Zolla, R. Petit, and M. Cadilhac, "Electromagnetic theory of diffraction by a system of parallel rods: The method of fictitious sources," *J. Opt. Soc. Amer. A*, vol. 11, no. 3, pp. 1087–1096, 1994.
[13] A. Madrazo and M. Nieto-Vesperinas, "Scattering of electromagnetic waves from a cylinder in front of a conducting plane," *J. Opt. Soc. Amer. A*, vol. 12, no. 6, pp. 1298–1309, 1995.
[14] R. Borghi, F. Gori, M. Santarsiero, F. Frezza, and G. Schettini, "Plane-wave scattering by a perfectly conducting circular cylinder near a plane surface: Cylindrical-wave approach," *J. Opt. Soc. Amer. A*, vol. 13, no. 3, pp. 483–493, 1996.
[15] R. Borghi, F. Gori, M. Santarsiero, F. Frezza, and G. Schettini, "Plane-wave scattering by a set of perfectly conducting circular cylinders in the presence of a plane surface," *J. Opt. Soc. Amer. A*, vol. 13, no. 12, pp. 2441–2452, 1996.
[16] T. Masuda and Y. Miyazaki, "Analysis of plane wave scattering by a conducting elliptic cylinder near a ground plane," in *Proc. IEEE Int. Symp. Electromagn. Compat.*, 1999, pp. 292–295.
[17] Y. Wang, Y. Zhang, M. He, and L. Guo, "Calculation of electromagnetic scattering from a two-dimensional target in the vicinity of a plane surface by a hybrid method," *J. Opt. Soc. Amer. A*, vol. 25, no. 6, pp. 1232–1239, 2008.
[18] S. Varault, S. Bolioli, and J. Sokoloff, "Scattering by an array of rods using the gaussian beam formalism coupled to the scattering matrix method," *J. Electromagn. Waves Appl.*, vol. 25, nos. 8–9, pp. 1131–1145, 2011.
[19] C. Ozzaim, "Plane wave scattering by a conducting cylinder located near an interface between two dielectric half-spaces: A perturbation method," *IEEE Trans. Antennas Propag.*, vol. 65, no. 5, pp. 2754–2758, May 2017.
[20] P. L. Uslenghi, "Scattering by two parallel metal wires over a conducting ground plane," in *Proc. IEEE Int. Conf. Electromagn. Adv. Appl. (ICEAA)*, 2018, pp. 5–7.
[21] A. Altaf, H. Sajjad, C. Ozzaim, and E. Arvas, "Scattering from chiral cylinders of arbitrary cross-sections above a ground plane," *IEEE Access*, vol. 9, pp. 6735–6745, 2021.
[22] H. Sajjad, A. Altaf, C. Ozzaim, and E. Arvas, "Scattering by a chiral cylinder of arbitrary cross section above a dielectric half-space," *IEEE Antennas Wireless Propag. Lett.*, vol. 20, pp. 778–782, 2021.
[23] J. Rubio, J. R. Mosig, R. Gómez-Alcalá, and M. A. G. de Aza, "Scattering by arbitrary cross-section cylinders based on the T-matrix approach and cylindrical to plane waves transformation," *IEEE Trans. Antennas Propag.*, vol. 70, no. 8, pp. 6983–6991, Aug. 2022.
[24] A. Epstein and O. Rabinovich, "Unveiling the properties of metagratings via a detailed analytical model for synthesis and analysis," *Phys. Rev. Appl.*, vol. 8, no. 5, 2017, Art. no. 54037.
[25] Y. Li, X. Ma, X. Wang, G. Ptitcyn, M. Movahediqomi, and S. A. Tretyakov, "All-angle scanning perfect anomalous reflection by using passive aperiodic gratings," *IEEE Trans. Antennas Propag.*, vol. 72, no. 1, pp. 877–889, Jan. 2023.

[26] M. Di Renzo et al., "Smart radio environments empowered by reconfigurable intelligent surfaces: How it works, state of research, and the road ahead," *J. Sel. Areas Commun.*, vol. 38, no. 11, pp. 2450–2525, 2020.

[27] A. Diaz-Rubio, S. Kosulnikov, and S. A. Tretyakov, "On the integration of reconfigurable intelligent surfaces in real-world environments: A convenient approach for estimation reflection and transmission," *IEEE Antennas Propag. Mag.*, vol. 64, no. 4, pp. 85–95, Aug. 2022.

[28] F. Bilotti et al., "Reconfigurable intelligent surfaces as the key-enabling technology for smart electromagnetic environments," *Adv. Phys. X*, vol. 9, no. 1, 2024, Art. no. 2299543.

[29] Y. Kerzhner and A. Epstein, "Metagrating-assisted high-directivity sparse regular antenna arrays for scanning applications," *IEEE Trans. Antennas Propag.*, vol. 71, no. 1, pp. 650–659, Jan. 2022.

[30] P. Nayeri, F. Yang, and A. Z. Elsherbeni, *Reflectarray Antennas: Theory, Designs, and Applications*. Hoboken, NJ, USA: Wiley, 2018.

[31] G. M. Battaglia, T. Isernia, R. Palmeri, and A. F. Morabito, "Synthesis of orbital angular momentum antennas for target localization," *Radio Sci.*, vol. 58, no. 2, pp. 1–15, 2023.

[32] J. Hu, S. Bandyopadhyay, Y. H. Liu, and L. Y. Shao, "A review on metasurface: From principle to smart metadevices," *Front. Phys.*, vol. 8, Jan. 2021, Art. no. 586087.

[33] R. Palmeri and T. Isernia, "Volumetric invisibility cloaks design through spectral coverage optimization," *IEEE Access*, vol. 7, pp. 30860–30867, 2019.

[34] Á. F. Vaquero, E. Martinez-de-Rioja, M. Arrebola, J. A. Encinar, and M. Achour, "Smart Electromagnetic Skin to Enhance Near Field Coverage in mm-Wave 5G Indoor Scenarios," *IEEE Trans. Antennas Propag.*, vol. 72, no. 5, pp. 4311–4326, May 2024.

[35] R. Palmeri, M. T. Bevacqua, A. F. Morabito, and T. Isernia, "Design of artificial-material-based antennas using inverse scattering techniques," *IEEE Trans. Antennas Propag.*, vol. 66, no. 12, pp. 7076–7090, Dec. 2018.

[36] R. Palmeri and T. Isernia, "Inverse design of artificial materials based lens antennas through the scattering matrix method," *Electronics*, vol. 9, no. 4, p. 559, 2020.

[37] R. Palmeri and T. Isernia, "Inverse design of EBG waveguides through scattering matrices," *EPJ Appl. Metamater.*, vol. 7, p. 10, Jan. 2021.

[38] M. Kouroublakis, G. P. Zouros, and N. L. Tsitsas, "Shielding effectiveness of metamaterial cylindrical arrays via the method of auxiliary sources," *IEEE Trans. Antennas Propag.*, vol. 72, no. 7, pp. 5950–5960, Jul. 2024.

[39] L. Crocco, F. Cuomo, and T. Isernia, "Generalized scattering-matrix method for the analysis of two-dimensional photonic bandgap devices," *J. Opt. Soc. Amer. A*, vol. 24, no. 10, pp. A12–A22, 2007.

[40] W. C. Chew. *Waves and Fields in Inhomogenous Media*. Hoboken, NJ, USA: Wiley, 1999.

[41] D. S. Jones. *The Theory of Electromagnetism*. Amsterdam, The Netherlands: Elsevier, 2013.

[42] P. Debye, "Das Verhalten von Lichtwellen in der Nähe eines Brennpunktes oder einer Brennlinie," *Annalen der Physik*, vol. 335, no. 14, pp. 755–776, 1909.

[43] J. A. Stratton, *Electromagnetic Theory*. Hoboken, NJ, USA: Wiley, 2007.

[44] O. M. Bucci and T. Isernia, "Electromagnetic inverse scattering: Retrievable information and measurement strategies," *Radio Sci.*, vol. 32, no. 6, pp. 2123–2137, 1997.

[45] M. Bosiljevac, M. Casaletti, F. Caminita, Z. Sipus, and S. Maci, "Non-uniform metasurface Luneburg lens antenna design," *IEEE Trans. Antennas Propag.*, vol. 60, no. 9, pp. 4065–4073, Sep. 2012.

[46] N. Nikolic, G. James, A. Hellicar, and K. Greene, "Quarter-sphere Luneburg lens scanning antenna," in *Proc. 15th Int. Symp. Antenna Technol. Appl. Electromagn.*, 2012, pp. 25–28.

[47] O. Zetterstrom, N. J. Fonseca, and O. Quevedo-Teruel, "Compact half-Luneburg lens antenna based on a glide-symmetric dielectric structure," *IEEE Antennas Wireless Propag. Lett.*, vol. 21, pp. 2283–2287, 2022.

[48] A. Díaz-Rubio, V. S. Asadchy, A. Elsakka, and S. A. Tretyakov, "From the generalized reflection law to the realization of perfect anomalous reflectors," *Sci. Adv.*, vol. 3, no. 8, 2017, Art. no. e1602714.

[49] M. Abramowitz and I. A. Stegun, *Handbook of Mathematical Functions with Formulas, Graphs, and Mathematical Tables*, vol. 55. Washington, DC, USA: U.S. Govern. Print. Office, 1968.